Highlights

- Neural trajectories in the hippocampus exhibited greater variability during a working memory (WM) task compared to those in the entorhinal cortex and amygdala regions.

- The distance of neural trajectories between encoding and retrieval states in the hippocampus was memory-load dependent during a WM task.

- Hippocampal neural trajectories fluctuated between the encoding and retrieval states in a task-dependent manner during both baseline and sharp-wave ripple (SWR) periods.

- Hippocampal neural trajectories shifted from encoding to retrieval states during SWR period.

Hippocampal neural fluctuations between memory encoding and retrieval states during a working memory task in humans

Yusuke Watanabe[a,*], Yuji Ikegaya[b,c,d], Takufumi Yanagisawa[a,e]

[a]*Institute for Advanced Cocreation studies, Osaka University, 2-2 Yamadaoka, Suita, 565-0871, Osaka, Japan*
[b]*Graduate School of Pharmaceutical Sciences, The University of Tokyo, 7-3-1 Hongo, Tokyo, 113-0033, Japan*
[c]*Institute for AI and Beyond, The University of Tokyo, 7-3-1 Hongo, Tokyo, 113-0033, Japan*
[d]*Center for Information and Neural Networks, National Institute of Information and Communications Technology, 1-4 Yamadaoka, Suita City, 565-0871, Osaka, Japan*
[e]*Department of Neurosurgery, Osaka University Graduate School of Medicine, 2-2 Yamadaoka, Osaka, 565-0871, Japan*

Abstract

~~The working~~ Working memory (WM), ~~a cornerstone of many~~ critical to various cognitive functions, ~~holds complex neural mechanisms that are not yet~~ embodies intricate neural mechanisms which are not entirely understood. ~~Specifically, the involvement~~ Notably, the role of the hippocampus and sharp-wave ripple complexes (SWRs) – ~~rapid, coincident neural~~ coordinated, rapid neuronal events within the hippocampus – in WM tasks remains somewhat ~~uncertain, despite their established roles~~ ambiguous, notwithstanding their confirmed involvement in memory consolidation and retrieval. In our ~~current~~ present research, we ~~propose~~ posit that multiunit activity patterns within the hippocampus ~~interact~~ operate synergistically with SWRs, ~~thereby displaying unique~~ consequently exhibiting distinctive dynamics during WM tasks. ~~This study involved an extensive~~ Our study engaged in a comprehensive analysis of a dataset ~~obtained~~ derived from intracranial electroencephalogram recordings from the medial temporal ~~lobe~~ lobes (MTL) of nine ~~patients with epilepsy, while performing~~ epileptic patients executing an eight-second Sternberg task. Gaussian-process factor analysis was ~~employed to identify~~ utilized to pinpoint low-dimensional neural ~~representations~~vectors, or 'trajectories,' within the MTL during the WM task. We ~~found~~ discovered that the hippocampus ~~exhibited the most significant variations~~ showed the most pronounced variation in neural trajectories ~~compared~~ relative to the entorhinal cortex and the amygdala. ~~Interestingly, the divergence~~ Intriguingly, the deviation in trajectories between the encoding and retrieval phases was ~~memory load-dependent. More specifically~~seen to be dependent on memory load. Further, hippocampal trajectories ~~oscillated~~ showed oscillatory behavior during the retrieval phase, ~~revealing task-dependent~~ indicating task-related transitions between encoding and retrieval states, ~~encapsulating~~ and embracing both baseline and SWR episodes. These oscillations ~~moved~~ transitioned from encoding to retrieval states ~~correlating~~ in correlation with the SWRs. ~~Therefore~~Hence, these findings ~~emphasize the essential~~ underscore the crucial role of the hippocampus in ~~performing~~ tackling WM tasks and ~~suggest a compelling premise for further investigation~~propose an enticing hypothesis for future exploration: the functional state of the hippocampus ~~transitions~~ switches from encoding to retrieval during SWRs.

Keywords: working memory, WM, memory load, hippocampus, sharp-wave ripples, SWR, humans

Working memory (WM) ~~plays a crucial~~ serves a critical role in everyday life, ~~and its neural underpinnings remain an area of ongoing research~~with its neural foundations being an ongoing subject of study. The hippocampus, ~~notably integral to memory~~ , ~~continues to be a primary focus of this investigation~~ particularly crucial to memory function, remains central to this research [1] [2] [3] [4] [5] [6] [7] [8] [9]. ~~Gaining insights into~~ Understanding the role of the hippocampus in working memory is ~~vital to deepening our understanding~~ essential to advancing our

*Corresponding author. Tel: +81-6-6879-3652

comprehension of cognitive processes, ~~hence fostering the progression of~~ thereby promoting cognitive training and interventions.

Current evidence ~~suggests a transient~~points toward a brief, synchronized oscillation, ~~referred to~~ known as sharp-wave ripple (SWR) [10], ~~is linked~~ being associated with several cognitive functions~~, such as~~. These include memory replay [11] [12] [13] [14] [15], memory consolidation [16] [17] [18] [19], memory recall [20] [21] [22], and neural plasticity [23] [24]. This ~~evidence indicates the likelihood that SWR could be a critical component of~~ suggests that SWR may play a crucial part in hippocampal processing, contributing to ~~working memory performance~~the performance of working memory. However, ~~research~~ studies investigating the effects of SWRs on working memory ~~remains sparse [25], and is largely limited to rodent models participating~~ are limited [25] and focus primarily on rodent models engaged in navigation tasks~~where the timing~~, without clear delineation of memory acquisition and recall ~~is not explicitly distinguished~~timing.

Recent studies ~~indicate~~ have illustrated that hippocampal neurons ~~exhibit~~ present low-dimensional representations during WM tasks. ~~Notably~~Specifically, the firing patterns of place cells [26] [27] [28] [29] [30], located in the hippocampus, ~~are observed to be encompassed~~ appear within a dynamic, nonlinear three-dimensional hyperbolic geometry in ~~rodents [31]. Moreover~~rodent models [31]. Additionally, grid cells in the entorhinal cortex (EC)—the ~~dominant pathway~~ main route to the hippocampus [32] [33] [34]—~~displayed~~ display a toroidal topology during exploration [35]. ~~Unfortunately, these investigations are confined~~ Regrettably, these studies are limited to spatial navigation tasks in rodents, ~~thus imposing limitations on~~ affecting the temporal resolution of WM tasks. The ~~applicability~~ application of these findings to human subjects and their ~~generalization~~ extension beyond navigation tasks ~~remains to be established~~are still unconfirmed.

~~Given these considerations, the current study aims to validate~~ In light of these points, the present study seeks to corroborate the hypothesis that hippocampal neurons ~~exhibit distinctive~~ portray unique representations in low-dimensional spaces, ~~designated~~ referred to as 'neural trajectory,' ~~during WM tasks, most prominently within SWR periods . To evaluate this claim, we employed a dataset of~~ particularly during SWR periods in WM tasks. To test this proposition, we used a dataset from patients performing an eight-second Sternberg task ~~with high temporal resolution~~ (1 ~~s~~ second for fixation, 2 ~~s~~ seconds for encoding, 3 ~~s~~ seconds for maintenance, and 2 ~~s~~ seconds for retrieval) with a high temporal resolution, while their intracranial electroencephalography ~~signals~~ (iEEG) ~~within~~ signals in the medial temporal lobe (MTL) were ~~being~~ monitored [36]. To ~~investigate~~ explore the low-dimensional neural trajectories, we ~~employed~~ utilized the Gaussian-process factor analysis (GPFA), a ~~method renowned for analyzing~~ recognized technique for examining neural population dynamics [37].

1. Methods

1.1. Dataset

A ~~publicly available dataset [36] was used, which consists of~~ public dataset [36] comprising experiments from nine epilepsy patients ~~performing~~ was taken into consideration for this study. The patients were tasked with executing a modified Sternberg task ~~. This task involves~~ which included four phases: fixation (1s), encoding (2s), maintenance (3s), and retrieval (2s) [36]. During the encoding phase, participants were ~~exposed to~~ presented with four, six, or eight alphabet letters, ~~referred to~~ known as the set size. Subsequently, they had to ~~decide~~ ascertain whether a probe letter ~~presented~~ revealed during the retrieval phase was ~~previously displayed (the correct~~ displayed earlier (the suitable choice for the Match IN task) or not (the ~~correct~~ suitable choice for the Mismatch OUT task). iEEG signals were ~~recorded at~~ registered via a sampling rate of 32 kHz, within a frequency ~~range~~ spectrum of 0.5–5,000 Hz, ~~using~~ utilizing depth electrodes implanted in the medial temporal lobe (MTL) regions: the anterior head of the left and ~~the~~ right hippocampus (AHL and AHR), the posterior body of the hippocampus (PHL and PHR), the entorhinal cortex (ECL and ECR), and the amygdala (AL and AR) ~~, as illustrated in~~ (Figure 1A and Table 1~~. The~~). The recorded iEEG signals were subsequently downsampled to a rate of 2 kHz. ~~Correlations~~ The interrelationship among variables such as set size and correct rate were ~~investigated~~ explored (Figure **??**S1). The timings of multiunit spikes were ~~determined by~~ identified using a spike sorting algorithm [38] ~~using~~

with the Combinato package (`https://github.com/jniediek/combinato`) (Figure 1C).

1.2. Calculation of neural trajectories using GPFA

Neural trajectories, ~~also termed~~ colloquially called 'factors' (Figure 1D), in the hippocampus, EC, and amygdala (Figure 1D) ~~, were computed using GPFA [37]~~were calculated utilizing GPFA [37], which was applied to the multiunit activity data ~~for~~ radiating from each session. ~~GPFA was~~ The computations were performed with the elephant package (`https://elephant.readthedocs.io/en/latest/reference/gpfa.html`). The bin size was set ~~to~~ at 50 ms, with no overlaps. Each factor was z-normalized across all sessions. The Euclidean distance from the origin (O) was ~~then~~ subsequently calculated (Figure 1E).

For each trajectory ~~within~~ inside a region, for ~~instance~~example, AHL, *geometric medians* (~~i.e.,~~ g_F for fixation, g_E for encoding, g_M for maintenance, and g_R for retrieval phase) were ~~determined by calculating~~ calculated by finding the median coordinates of the trajectory during the four phases (Figure 1D). An optimal dimensionality for GPFA was identified as three using the elbow method, which was derived by investigating the log-likelihood values through a three-fold cross-validation ~~approach~~ technique (Figure 2B).

1.3. Identifying SWR candidates from ~~hippocampal regions~~areas of the hippocampus

Potential SWR ~~events~~ instances from within the hippocampus were ~~detected using a widely~~ identified via an accepted method [39]. LFP signals from a given region of interest (ROI), such as AHL, were re-referenced by subtracting ~~an averaged~~ a calculated average signal from locations outside the ROI (~~*e.g.*~~e.g., AHR, PHL, PHR, ECL, ECR, AL, and AR) (see Figure 1A). The re-referenced LFP signals were ~~then~~ further filtered with a ripple-band filter (80–140 Hz) to ~~identify~~ detect SWR candidates (=SWR^+ candidates) (see Figure 1B). SWR detection was ~~conducted~~ carried out using a published tool (`https://github.com/Eden-Kramer-Lab/ripple_detection`) [40], with the bandpass range adjusted to 80–140 Hz ~~for humans~~ in line with human requirements [21] [22], ~~different from the original~~ as opposed to the conventional 150–250 Hz range typically applied to rodents.

Control events for SWR^+ candidates, ~~labeled~~ tagged as SWR^- candidates, were identified by ~~randomly~~ shuffling the timestamps of SWR^+ candidates randomly across all trials and subjects. The ~~resulting~~ resultant SWR^+/SWR^- candidates ~~were then subjected to visual inspection , as shown in~~ underwent visual inspection (Figure 1).

1.4. Defining SWRs from ~~putative~~ alleged hippocampal CA1 regions

SWRs were distinguished from SWR candidates ~~in presumptive~~ within likely CA1 regions. Initially, these regions were ~~defined~~ designated as follows: SWR^+/SWR^- candidates ~~in~~ from the hippocampus were ~~projected~~ mapped into a two-dimensional space based on the overlapping spike counts per unit ~~employing a supervised method using~~ using a supervised UMAP (Uniform Manifold Approximation and Projection) [41] (Figure 4A). ~~Clustering validation was performed~~ Validation of the clustering was done by computing the silhouette score [42] from the clustered samples (Table 2). ~~Regions~~ Those areas in the hippocampus ~~, which scored above~~ scoring over 0.6 on average across sessions (or the 75th percentile) ~~(Figure 4B), were characterized as presumed~~ were specified as likely CA1 regions, in turn, identifying five electrode positions ~~from five patients~~ across five participants (Table 3).

Those SWR^+/SWR^- candidates ~~in~~ within the assumed CA1 regions were classified as SWR^+/SWR^- ~~,~~ ~~thus relinquishing~~ and had their candidate status ~~. The~~ revoked. Log-normal distributions were observed in the duration and ripple band peak amplitude of SWRs ~~were observed to follow log-normal distributions~~ (Figure 44C ~~&~~ E). Each ~~time period of SWR~~ SWR time period was partitioned relative to the time from the SWR center into pre- (at −800 to −300 ms from SWR center), mid- (at −250 to +250 ms), and ~~post-SWR~~ post- (at +300 to +800 ms) SWR times.

1.5. Statistical evaluation

The Brunner–Munzel test and the Kruskal-Wallis test were performed using the SciPy package in Python [43]. ~~Correlational analysis was performed~~ A correlation analysis was executed by determining the rank of the ~~observed~~ correlation coefficient in its associated set-size-shuffled surrogate using a custom Python script.

The bootstrap test was ~~implemented using~~ conducted with an in-house Python script.

2. Results

2.1. *iEEG recording and neural trajectory in MTL regions during a Sternberg task*

We ~~leveraged~~ analyzed a publicly available dataset for this ~~analysis~~ study [36]. This dataset ~~encompasses~~ consists of LFP signals (Figure 1A) from MTL regions (Table 1) obtained during a modified Sternberg task ~~execution~~performance. We identified SWR^+ candidates from LFP signals filtered through the 80–140 Hz ripple band (Figure 1B) ~~, originating~~ across all hippocampal regions (refer to Methods). Correspondingly, SWR^- candidates were defined at ~~identical timestamps) but shuffled across~~ the same timestamps but shuffled between different trials (Figure 1). The dataset included multiunit spikes (Figure 1C) identified via a spike sorting algorithm [38]. ~~By employing~~ Using GPFA [37], and ~~using the~~ 50-ms binned multiunit activity ~~with no~~ without overlaps, we determined the neural trajectories (or factors) of MTL regions ~~by~~ per session and region (Figure 1D). We normalized each factor by session and region, for instance, session #2 in AHL of subject #1. Subsequently, we calculated the Euclidean distance from the origin (O) (Figure 1E).

2.2. *~~Hippocampal~~ Correlation between hippocampal neural trajectory ~~correlation with a~~ and Sternberg task performance*

Figure 2A ~~illustrates~~ shows the cloud of median neural trajectories of 50 trials within the three main factor spaces. We determined the optimal embedding dimension for the GPFA model to be three, using the elbow method (Figure 2B). The trajectory distance from the origin (O) (represented as $\|g_F\|$, $\|g_E\|$, $\|g_M\|$, and $\|g_R\|$) in the hippocampus ~~exceeded~~ was greater than the corresponding distances in the EC and amygdala (Figures 2C and D).[1]

Similarly, we ~~computed~~ calculated the distances between the geometric medians of the four phases, namely $\|g_F g_E\|$, $\|g_F g_M\|$, $\|g_F g_R\|$, $\|g_E g_M\|$, $\|g_E g_R\|$, and $\|g_M g_R\|$. The results indicated that the hippocampus ~~displayed~~ showed larger distances between phases than both the EC and amygdala. [2]

2.3. *Memory ~~load-dependent~~ load-dependence of neural trajectory distance between encoding and retrieval states in the hippocampus*

In ~~terms~~ the context of memory load in the ~~Stenberg~~ Sternberg task, we ~~identified~~ found a negative correlation between the correct rate of trials and set size (the number of letters to encode) (Figure 3A).[3] Similarly, we observed a positive correlation ~~was observed~~ between the response time and set size (Figure 3B).[4].

~~Furthermore, we found~~ Additionally, we observed a positive correlation between set size and the trajectory distance between the encoding and retrieval phases ($\log_{10}\|g_E g_R\|$) (Figure 3C).[5]. However, the distances between other combinations of phases did not ~~display statistically~~ show significant correlations (Figures 3D and S2).

2.4. *Detection of hippocampal SWR from putative CA1 regions*

~~For precision improvement in~~ To better localize recording sites and improve SWR detection, we estimated the electrode ~~placements~~ position in the CA1 regions of the hippocampus using distinct multiunit spike patterns during ~~the~~ SWR events. We embedded SWR^+/SWR^- candidates from ~~every~~ each session

[1] Hippocampus: Distance = 1.11 [1.01], median [IQR], n = 195,681 timepoints; EC: Distance = 0.94 [1.10], median [IQR], n = 133,761 timepoints; Amygdala: Distance = 0.78 [0.88], median [IQR], n = 165,281 timepoints.

[2] Hippocampus: Distance = 0.60 [0.70], median [IQR], n = 8,772 combinations; EC: Distance = 0.28 [0.52], median [IQR], n = 5,017 combinations ($p < 0.01$; Brunner–Munzel test); Amygdala: Distance = 0.24 [0.42], median [IQR], n = 7,466 combinations ($p < 0.01$; Brunner–Munzel test).

[3] Correct rate: set size four (0.99 ±0.11, mean ±SD; n = 333 trials) vs. set size six (0.93 ±0.26; n = 278 trials; $p < 0.001$, Brunner–Munzel test with Bonferroni correction) and set size eight (0.87 ±0.34; n = 275 trials; $p < 0.05$; Brunner–Munzel test with Bonferroni correction). Overall, $p < 0.001$ for Kruskal–Wallis test; correlation coefficient = -0.20, $p < 0.001$.

[4] Response time: set size four (1.26 ±0.45 s; n = 333 trials) vs. set size six (1.53 ±0.91 s; n = 278 trials) and set size eight (1.66 ±0.80 s; n = 275 trials). All comparisons $p < 0.001$, Brunner–Munzel test with Bonferroni correction; $p < 0.001$ for Kruskal–Wallis test; correlation coefficient = 0.22, $p < 0.001$

[5] Correlation between set size and $\log_{10}(\|g_E g_R\|)$: correlation coefficient = 0.05, $p < 0.001$. Specific values: $\|g_E g_R\|$ = 0.54 [0.70] for set size four, n = 447; $\|g_E g_R\|$ = 0.58 [0.66] for set size six, n = 381; $\|g_E g_R\|$ = 0.61 [0.63] for set size eight, n = 395.

and hippocampal region ~~were embedded~~ in a two-dimensional space ~~using~~ via UMAP (Figure 4A).[6] ~~We used~~ The quality of clustering was verified using the silhouette score as a metric ~~for quality of clustering~~ (Figure 4B and Table 2). Recording sites ~~with~~ yielding an average silhouette score ~~exceeding~~ over 0.6 across all sessions were ~~identified~~ designated as putative CA1 regions.[7] (Tables 2 and 3). We ~~identified~~ found five putative CA1 regions, ~~four of which were not~~ out of which four weren't labeled as seizure onset zones (Table 1).

~~Subsequently,~~ We further labeled SWR^+/SWR^- candidates within these putative CA1 regions ~~were labeled~~ as SWR^+ and SWR^-, respectively[8] (Table 3). Both SWR^+ and SWR^- exhibited ~~the same duration~~equal duration[9] (Figure 4C) due to their definitions, and ~~followed~~ adopted a log-distribution. ~~We observed an augmentation~~ There was an increase in SWR^+ incidence ~~during the initial~~ within the first 400 ms of the retrieval phase[10] (Figure 4D). The peak ripple band amplitude of SWR^+ ~~outpaced~~ was greater than that of SWR^- and followed a log-normal distribution (Figure 4E).[11].

2.5. Transient changes in hippocampal neural ~~trajectory~~ trajectories during SWR events

We ~~computed~~ calculated the distance of the trajectory from the origin (O) during SWR events in both the encoding and retrieval phases (Figure 5A). Observing ~~the~~ an increase in distance during SWR as shown in Figure 5A, we ~~differentiated~~ classified each SWR into three stages: pre-, mid-, and post-SWR. ~~Therefore~~Consequently, the distances from O during ~~those SWR periods are identified~~ these SWR stages are denoted as $\|\text{pre-eSWR}^+\|$, $\|\text{mid-eSWR}^+\|$ among others. The $\|\text{mid-eSWR}^+\|$[12] was ~~greater~~ larger than $\|\text{pre-eSWR}^+\|$[13], and $\|\text{mid-rSWR}^+\|$[14] was ~~larger~~ bigger than $\|\text{pre-rSWR}^+\|$ in both Match IN and Mismatch OUT tasks.[15].

2.6. Visualization of hippocampal neural ~~trajectory~~ trajectories during SWR in two-dimensional spaces

Following our observations ~~of~~ on neural trajectory 'jumping' during ~~SWR~~ a SWR event (Figure 5), we visualized the three-dimensional trajectories of pre-, mid-, and post-SWR events during the encoding and retrieval phases (Figure 6), the distance between which was found to ~~be memory-load dependent~~ depend on memory load (Figure 3).

To ~~provide~~ enable two-dimensional visualization, we linearly aligned peri-SWR trajectories by assigning g_E at the origin (0, 0) and g_R at ($\|g_E g_R\|$, 0). ~~Post this, we~~ We then rotated these aligned trajectories around the $g_E g_R$ axis (the x-axis). ~~Thus,~~ This method ensured that the distances from the origin in the original three-dimensional spaces ~~are~~ were preserved in the two-dimensional ~~equivalent~~counterparts.

The scatter plot within these two-dimensional spaces ~~reveals~~ illustrate characteristic distributions of peri-SWR trajectories based on ~~phases and task types . For instance, one can observe~~the phases and types of task. One can observe, for example, that the magnitude of $\|\text{mid-eSWR}^+\|$ surpasses that of $\|\text{pre-eSWR}^+\|$ (Figure 6B), which is consistent with our earlier findings (Figure 5).

2.7. ~~Fluctuations~~ Directionality of hippocampal neural trajectories between encoding and retrieval states

~~Next, we examined trajectory~~ We then investigated the *directions* of the trajectories in relation to $\overrightarrow{g_E g_R}$. The directions of SWRs were defined by the neural trajectory at −250 ms and +250 ms from their center, ~~i.e.,~~ namely $\overrightarrow{\text{eSWR}^+}$.

We calculated the density of $\overrightarrow{\text{eSWR}} \cdot \overrightarrow{g_E g_R}$, $\overrightarrow{\text{rSWR}} \cdot \overrightarrow{g_E g_R}$, and $\overrightarrow{\text{eSWR}} \cdot \overrightarrow{\text{rSWR}}$ (Figures 7A–D). The $\overrightarrow{\text{rSWR}^-} \cdot$

[6] Consider the AHL in session #1 of subject #1, for illustration purposes.

[7] The ~~identified~~ designated regions were: AHL of subject #1, AHR of subject #3, PHL of subject #4, AHL of subject #6, and AHR of subject #9.

[8] These definitions ~~led to~~ resulted in equal counts for both categories: SWR^+ (n = 1,170) and SWR^- (n = 1,170).

[9] These definitions ~~led to~~ resulted in equal durations for both categories: SWR^+ (93.0 [65.4] ms) and SWR^- (93.0 [65.4] ms).

[10] The occurrence of SWR^+ increased against the bootstrap sample; 95th percentile = 0.42 [Hz]; $p < 0.05$.

[11] SWR^+ (3.05 [0.85] SD of baseline, median [IQR]; n = 1,170) vs. SWR^- (2.37 [0.33] SD of baseline, median [IQR]; n = 1,170; $p < 0.001$; Brunner–Munzel test).

[12] 1.25 [1.30], median [IQR], n = 1,281, in Match IN task; 1.12 [1.35], median [IQR], n = 1,163, in Mismatch OUT task

[13] 1.08 [1.07], median [IQR], n = 1,149, in Match IN task; 0.90 [1.12], median [IQR], n = 1,088, in Mismatch OUT task

[14] 1.32 [1.24], median [IQR], n = 935, in Match IN task; 1.15 [1.26], median [IQR], n = 891, in Mismatch OUT task

[15] 1.19 [0.96], median [IQR], n = 673, in Match IN task; 0.94 [0.88], median [IQR], n = 664, in Mismatch OUT task

$\overrightarrow{g_E g_R}$ ~~displayed~~ demonstrated a biphasic distribution.

By ~~taking the difference between~~ comparing the distribution of $\overrightarrow{rSWR^+} \cdot \overrightarrow{g_E g_R}$ (Figures 7A and B) ~~and~~ with that of $\overrightarrow{rSWR^-} \cdot \overrightarrow{g_E g_R}$ (Figures 7C and D), we computed the contributions of SWR (Figures 7E and F), which ~~revealed~~ indicated a shift in the direction of $\overrightarrow{g_E g_R}$ (Figures 7E and F: *red rectangles*).

~~Moreover, exclusively~~ Furthermore, and only in the Mismatch OUT task, $\overrightarrow{eSWR^+} \cdot \overrightarrow{rSWR^+}$ was less than $\overrightarrow{eSWR^-} \cdot \overrightarrow{rSWR^-}$ (baseline periods) (Figure 7F: *pink circles*). ~~In simpler terms~~Put simply, eSWR and rSWR pointed in ~~the opposite direction~~ opposite directions only in the Mismatch OUT task but not in the Match IN task (Figure 7E: *pink circles*).

3. Discussion

4. Discussion

This study ~~hypothesized that~~ posits that hippocampal neurons generate distinct trajectories within low-dimensional spaces during a working memory (WM) task in humans, ~~hippocampal neurons form unique trajectories, particularly~~ specifically during sharp-wave ripple (SWR) periods. Initially, ~~the~~ multiunit spikes in the medial temporal lobe (MTL) regions were projected onto three-dimensional spaces during a Sternberg task using Gaussian Process Factor Analysis (GPFA) (Figure 1D–E and Figure 2A). The ~~distance of the trajectory~~ trajectory distance across WM phases ($\|g_F g_E\|$, $\|g_F g_M\|$, $\|g_F g_R\|$, $\|g_E g_M\|$, $\|g_E g_R\|$, and $\|g_M g_R\|$) was ~~notably~~ markedly larger in the hippocampus than in the EC and amygdala (Figure 2E), ~~indicating~~ which implies dynamic neural activity in the hippocampus during the WM task. ~~Further~~Additionally, in the hippocampus, the trajectory distance between ~~the~~ encoding and retrieval phases ($\|g_F g_E\|$) ~~exhibited a positive correlation~~ was found to positively correlate with memory load (Figure 3C–D), ~~reflecting~~ denoting WM processing. The hippocampal neural trajectory ~~was found to increase transiently~~ momentarily increased during SWRs (Figure 5). ~~Finally~~Eventually, the hippocampal neural trajectory ~~switched~~ alternated between encoding and retrieval states, ~~moving~~ progressing specifically from encoding to retrieval during SWR events (Figure 7). ~~These findings not only explain various facets~~ Such discoveries not only interpret varying aspects of hippocampal neural activity during a WM task in humans, but also offer ~~new~~ fresh insights into how SWRs ~~influence the switch in~~ help alter neural states.

~~We found~~ Our findings show that the distance of ~~the~~ hippocampal neural trajectory across the phases~~was greater in the hippocampus compared to that in the EC and amygdala, even when~~ , even after considering the distance from O in these regions, surpassed that in the EC and amygdala (Figure 2C–E). This ~~supports the involvement~~ reaffirms the participation of the hippocampus in the WM task, ~~aligning with previous reports~~ coinciding with prior assertions of hippocampal persistent firing during the maintenance phase [3] [4] [5] [6]. However, when ~~we applied~~ applying GPFA to multiunit activity during a 1-second level resolution of the WM task, we ~~observed~~ noticed that the neural trajectory in low-dimensional space ~~showed~~ demonstrated a memory-load ~~dependency between the~~ dependence between encoding and retrieval phases, ~~symbolized~~ denoted as $\|g_E g_R\|$ (Figure 3). ~~These findings corroborate the association of the hippocampus with~~ This supports the association between the hippocampus and WM processing.

Our analysis ~~was confined to~~ focused on putative CA1 regions (Figure 4), which ~~was bolstered by several factors~~is supported by various contributions. This specific ~~focus stems from established observations that SWRs synchronize with spike bursts~~ concentration arises from well-established observations where SWRs coincide with spike clusters of interneurons and pyramidal neurons [44] [45] [46] [47], potentially within a 50 μm radius of the recording site [48]. ~~We further identified an increased incidence of SWRs~~ An increase in the instances of SWRs was identified during the first 0–400 ms of the retrieval phase (Figure 4D). This ~~finding harmonizes with previous reports of heightened SWR occurrence preceding~~ observation aligns with earlier reports of increased SWR occurrence before spontaneous verbal recall [21] [22], ~~supporting our results~~ reinforcing our findings under a triggered retrieval condition. The ~~observed~~ log-normal distributions of both SWR ~~duration~~ length and ripple band peak amplitude observed in this study (Figure 4C & E) ~~is in accordance with the consensus in this field[39]. As a result, our decision to restrict recording sites~~ concur with the field's consensus [39]. Consequently, confining

recordings to putative CA1 regions likely ~~contributed to enhancing~~ improved the accuracy of SWR detection. However, the observed increase in trajectory distance from *O* during SWRs (Figure 5) ~~might have been skewed towards higher values~~ may be skewed higher due to channel selection. ~~However~~Nevertheless, this potential bias does not ~~substantially challenge our primary findings~~significantly undermine our primary conclusions.

Interestingly, during the retrieval phase, ~~the trajectory directions oscillated~~ trajectory directions alternated between encoding and retrieval states ~~during both~~ both during baseline and SWR periods (Figure 7C & D). ~~Moreover~~Furthermore, the balance of this oscillation ~~shifted~~ transitioned from encoding to retrieval state during SWR ~~events~~ episodes (Figure 7 E & F). These ~~results are consistent with previous reports on~~ outcomes align with preceding reports regarding the role of ~~SWR~~ SWRs in memory retrieval [21] [22]. Our findings ~~highlight a new understanding , suggesting that~~ suggest a novel understanding where SWRs occur when the hippocampal representation transitions from encoding to retrieval states~~. Therefore, these results reveal novel~~ , thereby revealing unexplored aspects of hippocampal representations, ~~including~~ such as (i) neuronal oscillation between encoding and retrieval ~~states~~ phases during a WM task, and (ii) SWR ~~serving as a trigger~~ functioning as a catalyst for changing neural states.

~~Furthermore~~Moreover, our study ~~uncovered WM-task type-specific~~ identified differences between encoding- and retrieval-SWRs (Figure 7E–F) specific to WM-task types. Notably, ~~opposing~~ counter movements of encoding-SWR (eSWR) and retrieval-SWR (rSWR) were not ~~observed~~ seen in the Match IN task but were ~~apparent~~ evident in the Mismatch OUT task. ~~These observations can be explained by the~~ The memory engram theory ~~[49]. Particularly, the~~ can explain these observations [49]. The Match In task~~provided participants with previously presented letters, contrastingly,~~ , for instance, presented participants with previous letters, whereas the Mismatch OUT task introduced a new letter ~~not present~~ absent in the encoding phase. These interpretations ~~underscore the significant~~ highlight the vital role of SWR in human cognitive processes.

In conclusion, ~~the present~~ this investigation demonstrated that during a WM task, hippocampal activity oscillates between encoding and retrieval states~~during a WM task and uniquely transitions~~ , uniquely transitioning from encoding to retrieval during SWR ~~incidents~~events. These findings ~~provide meaningful insight~~ offer valuable insights into the neural ~~counterparts and functionality~~ substrates and workings of working memory ~~in~~ within the hippocampus.

References

[1] W. B. Scoville, B. Milner, LOSS OF RECENT MEMORY AFTER BILATERAL HIPPOCAMPAL LESIONS, Journal of Neurology, Neurosurgery, and Psychiatry 20 (1) (1957) 11–21. URL https://www.ncbi.nlm.nih.gov/pmc/articles/PMC497229/

[2] L. R. Squire, The Legacy of Patient H.M. for Neuroscience, Neuron 61 (1) (2009) 6–9. doi:10.1016/j.neuron.2008.12.023.
URL https://www.ncbi.nlm.nih.gov/pmc/articles/PMC2649674/

[3] E. Boran, T. Fedele, P. Klaver, P. Hilfiker, L. Stieglitz, T. Grunwald, J. Sarnthein, Persistent hippocampal neural firing and hippocampal-cortical coupling predict verbal working memory load, Science Advances 5 (3) (2019) eaav3687. doi:10.1126/sciadv.aav3687.
URL https://www.science.org/doi/10.1126/sciadv.aav3687

[4] J. Kamiński, S. Sullivan, J. M. Chung, I. B. Ross, A. N. Mamelak, U. Rutishauser, Persistently active neurons in human medial frontal and medial temporal lobe support working memory, Nature Neuroscience 20 (4) (2017) 590–601, number: 4 Publisher: Nature Publishing Group. doi:10.1038/nn.4509.
URL https://www.nature.com/articles/nn.4509

[5] S. Kornblith, R. Q. Quiroga, C. Koch, I. Fried, F. Mormann, Persistent Single-Neuron Activity during Working Memory in the Human Medial Temporal Lobe, Current Biology 27 (7) (2017) 1026–1032, publisher: Elsevier. doi:10.1016/j.cub.2017.02.013.
URL https://www.cell.com/current-biology/abstract/S0960-9822(17)30149-5

[6] M. C. M. Faraut, A. A. Carlson, S. Sullivan, O. Tudusciuc, I. Ross, C. M. Reed, J. M. Chung, A. N. Mamelak, U. Rutishauser, Dataset of human medial temporal lobe single neuron activity during declarative memory encoding and recognition, Scientific Data 5 (1) (2018) 180010, number: 1 Publisher: Nature Publishing Group. doi:10.1038/sdata.2018.10.
URL https://www.nature.com/articles/sdata201810

[7] A. A. Borders, C. Ranganath, A. P. Yonelinas, The hippocampus supports high-precision binding in visual working memory, Hippocampus 32 (3) (2022) 217–230. doi:10.1002/hipo.23401.

[8] J. Li, D. Cao, S. Yu, X. Xiao, L. Imbach, L. Stieglitz, J. Sarnthein, T. Jiang, Functional specialization and interaction in the amygdala-hippocampus circuit during working memory processing, Nature Communications 14 (1) (2023)

2921, number: 1 Publisher: Nature Publishing Group. doi:10.1038/s41467-023-38571-w.
URL https://www.nature.com/articles/s41467-023-38571-w

[9] V. Dimakopoulos, P. Mégevand, L. H. Stieglitz, L. Imbach, J. Sarnthein, Information flows from hippocampus to auditory cortex during replay of verbal working memory items, eLife 11 (2022) e78677, publisher: eLife Sciences Publications, Ltd. doi:10.7554/eLife.78677.
URL https://doi.org/10.7554/eLife.78677

[10] G. Buzsáki, Hippocampal sharp wave-ripple: A cognitive biomarker for episodic memory and planning, Hippocampus 25 (10) (2015) 1073–1188, _eprint: https://onlinelibrary.wiley.com/doi/pdf/10.1002/hipo.22488. doi:https://doi.org/10.1002/hipo.22488.
URL https://onlinelibrary.wiley.com/doi/abs/10.1002/hipo.22488

[11] M. A. Wilson, B. L. McNaughton, Reactivation of hippocampal ensemble memories during sleep, Science (New York, N.Y.) 265 (5172) (1994) 676–679. doi:10.1126/science.8036517.

[12] Z. Nádasdy, H. Hirase, A. Czurkó, J. Csicsvari, G. Buzsáki, Replay and Time Compression of Recurring Spike Sequences in the Hippocampus, Journal of Neuroscience 19 (21) (1999) 9497–9507, publisher: Society for Neuroscience Section: ARTICLE. doi:10.1523/JNEUROSCI.19-21-09497.1999.
URL https://www.jneurosci.org/content/19/21/9497

[13] A. K. Lee, M. A. Wilson, Memory of sequential experience in the hippocampus during slow wave sleep, Neuron 36 (6) (2002) 1183–1194. doi:10.1016/s0896-6273(02)01096-6.

[14] K. Diba, G. Buzsáki, Forward and reverse hippocampal place-cell sequences during ripples, Nature Neuroscience 10 (10) (2007) 1241–1242, number: 10 Publisher: Nature Publishing Group. doi:10.1038/nn1961.
URL https://www.nature.com/articles/nn1961

[15] T. J. Davidson, F. Kloosterman, M. A. Wilson, Hippocampal replay of extended experience, Neuron 63 (4) (2009) 497–507. doi:10.1016/j.neuron.2009.07.027.

[16] G. Girardeau, K. Benchenane, S. I. Wiener, G. Buzsáki, M. B. Zugaro, Selective suppression of hippocampal ripples impairs spatial memory, Nature Neuroscience 12 (10) (2009) 1222–1223. doi:10.1038/nn.2384.
URL http://www.nature.com/articles/nn.2384

[17] V. Ego-Stengel, M. A. Wilson, Disruption of ripple-associated hippocampal activity during rest impairs spatial learning in the rat, Hippocampus 20 (1) (2010) 1–10. doi:10.1002/hipo.20707.

[18] A. Fernández-Ruiz, A. Oliva, E. Fermino de Oliveira, F. Rocha-Almeida, D. Tingley, G. Buzsáki, Long-duration hippocampal sharp wave ripples improve memory, Science (New York, N.Y.) 364 (6445) (2019) 1082–1086. doi:10.1126/science.aax0758.
URL https://www.ncbi.nlm.nih.gov/pmc/articles/PMC6693581/

[19] J. Kim, A. Joshi, L. Frank, K. Ganguly, Cortical–hippocampal coupling during manifold exploration in motor cortex, Nature (2022) 1–8Publisher: Nature Publishing Group. doi:10.1038/s41586-022-05533-z.
URL https://www.nature.com/articles/s41586-022-05533-z

[20] C.-T. Wu, D. Haggerty, C. Kemere, D. Ji, Hippocampal awake replay in fear memory retrieval, Nature Neuroscience 20 (4) (2017) 571–580. doi:10.1038/nn.4507.

[21] Y. Norman, E. M. Yeagle, S. Khuvis, M. Harel, A. D. Mehta, R. Malach, Hippocampal sharp-wave ripples linked to visual episodic recollection in humans, Science 365 (6454) (2019) eaax1030. doi:10.1126/science.aax1030.
URL https://www.sciencemag.org/lookup/doi/10.1126/science.aax1030

[22] Y. Norman, O. Raccah, S. Liu, J. Parvizi, R. Malach, Hippocampal ripples and their coordinated dialogue with the default mode network during recent and remote recollection, Neuron 109 (17) (2021) 2767–2780.e5, publisher: Elsevier. doi:10.1016/j.neuron.2021.06.020.
URL https://www.cell.com/neuron/abstract/S0896-6273(21)00461-X

[23] C. J. Behrens, L. P. van den Boom, L. de Hoz, A. Friedman, U. Heinemann, Induction of sharp wave–ripple complexes in vitro and reorganization of hippocampal networks, Nature Neuroscience 8 (11) (2005) 1560–1567, number: 11 Publisher: Nature Publishing Group. doi:10.1038/nn1571.
URL https://www.nature.com/articles/nn1571

[24] H. Norimoto, K. Makino, M. Gao, Y. Shikano, K. Okamoto, T. Ishikawa, T. Sasaki, H. Hioki, S. Fujisawa, Y. Ikegaya, Hippocampal ripples down-regulate synapses, Science (New York, N.Y.) 359 (6383) (2018) 1524–1527. doi:10.1126/science.aao0702.

[25] S. P. Jadhav, C. Kemere, P. W. German, L. M. Frank, Awake Hippocampal Sharp-Wave Ripples Support Spatial Memory, Science 336 (6087) (2012) 1454–1458, publisher: American Association for the Advancement of Science. doi:10.1126/science.1217230.
URL https://www.science.org/doi/abs/10.1126/science.1217230

[26] J. O'Keefe, J. Dostrovsky, The hippocampus as a spatial map: Preliminary evidence from unit activity in the freely-moving rat, Brain Research 34 (1971) 171–175, place: Netherlands Publisher: Elsevier Science. doi:10.1016/0006-8993(71)90358-1.

[27] J. O'Keefe, Place units in the hippocampus of the freely moving rat, Experimental Neurology 51 (1) (1976) 78–109. doi:10.1016/0014-4886(76)90055-8.
URL https://www.sciencedirect.com/science/article/pii/0014488676900558

[28] A. D. Ekstrom, M. J. Kahana, J. B. Caplan, T. A. Fields, E. A. Isham, E. L. Newman, I. Fried, Cellular networks underlying human spatial navigation, Nature 425 (6954) (2003) 184–188, number: 6954 Publisher: Nature Publishing Group. doi:10.1038/nature01964.
URL https://www.nature.com/articles/nature01964

[29] K. B. Kjelstrup, T. Solstad, V. H. Brun, T. Hafting, S. Leutgeb, M. P. Witter, E. I. Moser, M.-B. Moser, Finite Scale of Spatial Representation in the Hippocampus, Science 321 (5885) (2008) 140–143, publisher: American Association for the Advancement of Science. doi:10.1126/science.1157086.
URL https://www.science.org/doi/abs/10.1126/science.1157086

[30] C. D. Harvey, F. Collman, D. A. Dombeck, D. W. Tank, Intracellular dynamics of hippocampal place cells during virtual navigation, Nature 461 (7266) (2009) 941–946, number: 7266 Publisher: Nature Publishing Group. doi:10.1038/nature08499.
URL https://www.nature.com/articles/nature08499

[31] H. Zhang, P. D. Rich, A. K. Lee, T. O. Sharpee, Hippocampal spatial representations exhibit a hyperbolic geometry that expands with experience, Nature Neuroscience (Dec. 2022). doi:10.1038/s41593-022-01212-4.
URL https://www.nature.com/articles/s41593-022-01212-4

[32] P. A. Naber, F. H. Lopes da Silva, M. P. Witter, Reciprocal connections between the entorhinal cortex and hippocampal fields CA1 and the subiculum are in register with the projections from CA1 to the subiculum, Hippocampus 11 (2) (2001) 99–104, _eprint: https://onlinelibrary.wiley.com/doi/pdf/10.1002/hipo.1028. doi:10.1002/hipo.1028.
URL https://onlinelibrary.wiley.com/doi/abs/10.1002/hipo.1028

[33] N. M. van Strien, N. L. M. Cappaert, M. P. Witter, The anatomy of memory: an interactive overview of the parahippocampal–hippocampal network, Nature Reviews Neuroscience 10 (4) (2009) 272–282, number: 4 Publisher: Nature Publishing Group. doi:10.1038/nrn2614.
URL https://www.nature.com/articles/nrn2614

[34] B. A. Strange, M. P. Witter, E. S. Lein, E. I. Moser, Functional organization of the hippocampal longitudinal axis, Nature Reviews Neuroscience 15 (10) (2014) 655–669, number: 10 Publisher: Nature Publishing Group. doi:10.1038/nrn3785.
URL https://www.nature.com/articles/nrn3785

[35] R. J. Gardner, E. Hermansen, M. Pachitariu, Y. Burak, N. A. Baas, B. A. Dunn, M.-B. Moser, E. I. Moser, Toroidal topology of population activity in grid cells, Nature 602 (7895) (2022) 123–128, number: 7895 Publisher: Nature Publishing Group. doi:10.1038/s41586-021-04268-7.
URL https://www.nature.com/articles/s41586-021-04268-7

[36] E. Boran, T. Fedele, A. Steiner, P. Hilfiker, L. Stieglitz, T. Grunwald, J. Sarnthein, Dataset of human medial temporal lobe neurons, scalp and intracranial EEG during a verbal working memory task, Scientific Data 7 (1) (2020) 30, number: 1 Publisher: Nature Publishing Group. doi:10.1038/s41597-020-0364-3.
URL https://www.nature.com/articles/s41597-020-0364-3

[37] B. M. Yu, J. P. Cunningham, G. Santhanam, S. I. Ryu, K. V. Shenoy, M. Sahani, Gaussian-Process Factor Analysis for Low-Dimensional Single-Trial Analysis of Neural Population Activity, Journal of Neurophysiology 102 (1) (2009) 614–635. doi:10.1152/jn.90941.2008.
URL https://www.ncbi.nlm.nih.gov/pmc/articles/PMC2712272/

[38] J. Niediek, J. Boström, C. E. Elger, F. Mormann, Reliable Analysis of Single-Unit Recordings from the Human Brain under Noisy Conditions: Tracking Neurons over Hours, PLOS ONE 11 (12) (2016) e0166598, publisher: Public Library of Science. doi:10.1371/journal.pone.0166598.
URL https://journals.plos.org/plosone/article?id=10.1371/journal.pone.0166598

[39] A. A. Liu, S. Henin, S. Abbaspoor, A. Bragin, E. A. Buffalo, J. S. Farrell, D. J. Foster, L. M. Frank, T. Gedankien, J. Gotman, J. A. Guidera, K. L. Hoffman, J. Jacobs, M. J. Kahana, L. Li, Z. Liao, J. J. Lin, A. Losonczy, R. Malach, M. A. van der Meer, K. McClain, B. L. McNaughton, Y. Norman, A. Navas-Olive, L. M. de la Prida, J. W. Rueckemann, J. J. Sakon, I. Skelin, I. Soltesz, B. P. Staresina, S. A. Weiss, M. A. Wilson, K. A. Zaghloul, M. Zugaro, G. Buzsáki, A consensus statement on detection of hippocampal sharp wave ripples and differentiation from other fast oscillations, Nature Communications 13 (1) (2022) 6000, number: 1 Publisher: Nature Publishing Group. doi:10.1038/s41467-022-33536-x.
URL https://www.nature.com/articles/s41467-022-33536-x

[40] K. Kay, M. Sosa, J. E. Chung, M. P. Karlsson, M. C. Larkin, L. M. Frank, A hippocampal network for spatial coding during immobility and sleep, Nature 531 (7593) (2016) 185–190. doi:10.1038/nature17144.

[41] L. McInnes, J. Healy, N. Saul, L. Großberger, UMAP: Uniform Manifold Approximation and Projection, Journal of Open Source Software 3 (29) (2018) 861. doi:10.21105/joss.00861.
URL https://joss.theoj.org/papers/10.21105/joss.00861

[42] P. J. Rousseeuw, Silhouettes: A graphical aid to the interpretation and validation of cluster analysis, Journal of Computational and Applied Mathematics 20 (1987) 53–65. doi:10.1016/0377-0427(87)90125-7.
URL https://www.sciencedirect.com/science/article/pii/0377042787901257

[43] P. Virtanen, R. Gommers, T. E. Oliphant, M. Haberland, T. Reddy, D. Cournapeau, E. Burovski, P. Peterson, W. Weckesser, J. Bright, S. J. van der Walt, M. Brett, J. Wilson, K. J. Millman, N. Mayorov, A. R. J. Nelson, E. Jones, R. Kern, E. Larson, C. J. Carey, Polat, Y. Feng, E. W. Moore, J. VanderPlas, D. Laxalde, J. Perktold, R. Cimrman, I. Henriksen, E. A. Quintero, C. R. Harris, A. M. Archibald, A. H. Ribeiro, F. Pedregosa, P. van Mulbregt, SciPy 1. 0 Contributors, SciPy 1.0: fundamental algorithms for scientific computing in Python, Nature Methods 17 (2020) 261–272, aDS Bibcode: 2020NatMe..17..261V. doi:10.1038/s41592-019-0686-2.
URL https://ui.adsabs.harvard.edu/abs/2020NatMe..17..261V

[44] G. Buzsáki, Two-stage model of memory trace formation: a role for "noisy" brain states, Neuroscience 31 (3) (1989) 551–570. doi:10.1016/0306-4522(89)90423-5.

[45] M. L. V. Quyen, A. Bragin, R. Staba, B. Crépon, C. L. Wilson, J. Engel, Cell Type-Specific Firing during Ripple Oscillations in the Hippocampal Formation of Humans, Journal of Neuroscience 28 (24) (2008) 6104–6110, publisher: Society for Neuroscience Section: Brief Communications. doi:10.1523/JNEUROSCI.0437-08.2008.
URL https://www.jneurosci.org/content/28/24/6104

[46] S. Royer, B. V. Zemelman, A. Losonczy, J. Kim, F. Chance, J. C. Magee, G. Buzsáki, Control of timing, rate and bursts of hippocampal place cells by dendritic and somatic inhibition, Na-

ture Neuroscience 15 (5) (2012) 769–775, number: 5 Publisher: Nature Publishing Group. doi:10.1038/nn.3077.
URL https://www.nature.com/articles/nn.3077

[47] N. Hájos, M. R. Karlócai, B. Németh, I. Ulbert, H. Monyer, G. Szabó, F. Erdélyi, T. F. Freund, A. I. Gulyás, Input-output features of anatomically identified CA3 neurons during hippocampal sharp wave/ripple oscillation in vitro, The Journal of Neuroscience: The Official Journal of the Society for Neuroscience 33 (28) (2013) 11677–11691. doi:10.1523/JNEUROSCI.5729-12.2013.

[48] E. W. Schomburg, C. A. Anastassiou, G. Buzsáki, C. Koch, The Spiking Component of Oscillatory Extracellular Potentials in the Rat Hippocampus, The Journal of Neuroscience 32 (34) (2012) 11798–11811. doi:10.1523/JNEUROSCI.0656-12.2012.
URL https://www.ncbi.nlm.nih.gov/pmc/articles/PMC3459239/

[49] X. Liu, S. Ramirez, P. T. Pang, C. B. Puryear, A. Govindarajan, K. Deisseroth, S. Tonegawa, Optogenetic stimulation of a hippocampal engram activates fear memory recall, Nature 484 (7394) (2012) 381–385, number: 7394 Publisher: Nature Publishing Group. doi:10.1038/nature11028.
URL https://www.nature.com/articles/nature11028

Contributors

Y.W. and T.Y. conceptualized the study; Y.W. performed the data analysis; Y.W. and T.Y. wrote the original draft; and all authors reviewed the final manuscript.

Acknowledgments

This research was funded by a grant from the Exploratory Research for Advanced Technology (JPMJER1801).

Declaration of Interests

The authors declare that they have no competing interests.

Data and code availability

The data is available on G-Node (https://doi.gin.g-node.org/10.12751/g-node.d76994/).
The source code is available on GitHub (https://github.com/yanagisawa-lab/hippocampal-neural-fluctuation-during-a-WM-task-in-humans).

Inclusion and Diversity Statement

We support inclusive, diverse, and equitable conduct of research.

Declaration of Generative AI in Scientific Writing

The authors employed ChatGPT, provided by OpenAI, for enhancing the manuscript's English language quality. After incorporating the suggested improvements, the authors meticulously revised the content. Ultimate responsibility for the final content of this publication rests entirely with the authors.

Tables

Subject ID	of sessions	AHL	AHR	PHL	PHR	ECL	ECR	AL	AR	SOZ
1	4	o	x	o	o	o	x	o	x	"AHR, LR"
2	7	o	o	o	o	o	o	o	o	"AHR, PHR"
3	3	o	o	o	o	o	o	o	x	"AHL, PHL"
4	2	o	o	o	o	o	o	o	o	"AHL, AHR, PHL, PHR"
5	3	o	x	x	o	x	x	o	x	DRR
6	6	o	o	o	o	o	o	o	o	"AHL, PHL, ECL, AL"
7	4	o	o	o	o	o	o	o	o	"AHR, PHR"
8	5	o	o	o	o	o	o	o	o	ECR
9	2	o	o	o	o	o	o	o	o	"ECR, AR"

Table 1 – ~~Distribution of Electrodes within the Dataset~~ Electrode Distribution within the Dataset

~~This~~ The figure ~~represents the~~ outlines electrode placements and ~~the~~ seizure onset zones. ~~Regions designated~~ Areas labelled with "o" ~~were available~~ are included in the dataset, ~~whereas~~ while those ~~marked with~~ indicated by "x" (*navy*) ~~were not present~~are absent. ~~Abbreviations include~~Denoted abbreviations: AHL, left hippocampal head; AHR, right hippocampal head; PHL, left hippocampal body; PHR, right hippocampal body; ECL, left entorhinal cortex; ECR, right entorhinal cortex; AL, left amygdala; AR, right amygdala~~; and~~ . SOZ ~~symbolizes~~ refers to the seizure onset zone.

Subject	AHL	AHR	PHL	PHR
1	0.60 ± 0.14	n.a.	n.a.	0.1 ± 0
2	0.21 ± 0.16	0.17 ± 0.21	0.18 ± 0.22	0.20 ± 0.15
3	0.40 ± 0.42	0.83 ± 0.12	n.a.	n.a.
4	0.10 ± 0.00	0.10 ± 0.00	0.90 ± 0.00	0.10 ± 0.14
5	n.a.	n.a.	n.a.	n.a.
6	0.63 ± 0.06	n.a.	n.a.	0.27 ± 0.06
7	0.10 ± 0.00	0.35 ± 0.35	0.37 ± 0.47	0.10 ± 0.00
8	0.13 ± 0.10	n.a.	0.28 ± 0.49	n.a.
9	n.a.	0.85 ± 0.07	0.15 ± 0.07	n.a.

Table 2 – ~~**Silhouette score of UMAP clustering for SWR^+ candidates and SWR^- candidates**~~ **Silhouette scores of UMAP clustering for SWR^+ candidates and SWR^- candidates**

The silhouette scores (mean ± SD across sessions per subject) ~~for~~ pertaining to UMAP clustering of SWR+ candidates and SWR candidates ~~(~~are calculated and presented in Figure 4A~~) were calculated~~. These calculations are based on their corresponding multiunit spike patterns~~(~~, where the mean values ~~were~~ observed are 0.205 with a standard deviation of 0.285~~,~~. The median ~~IQR;~~ and interquartile range are also presented (see Figure 4B).

Subject ID	of sessions	of trials	ROI	of SWRs	SWR incidence [Hz]
1	2	100	AHL	274	0.34
3	2	97	AHR	325	0.42
4	2	99	PHL	202	0.26
6	2	100	AHL	297	0.37
9	2	97	AHR	72	0.09
Total = 10	Total = 493	"Total = 1,170"	0.30 ± 0.13 (mean ± SD)		

Table 3 – ~~**Accounting for Defined SWR Events**~~ **Accounting for Specific SWR Events**

The table ~~collates~~ compiles statistics ~~of putative~~ related to assumed CA1 regions and SWR events. ~~Only~~ To minimize sampling bias, only the ~~first~~ initial two sessions (sessions 1 and 2) from each subject were ~~considered to minimize sampling bias~~utilized.

Figures

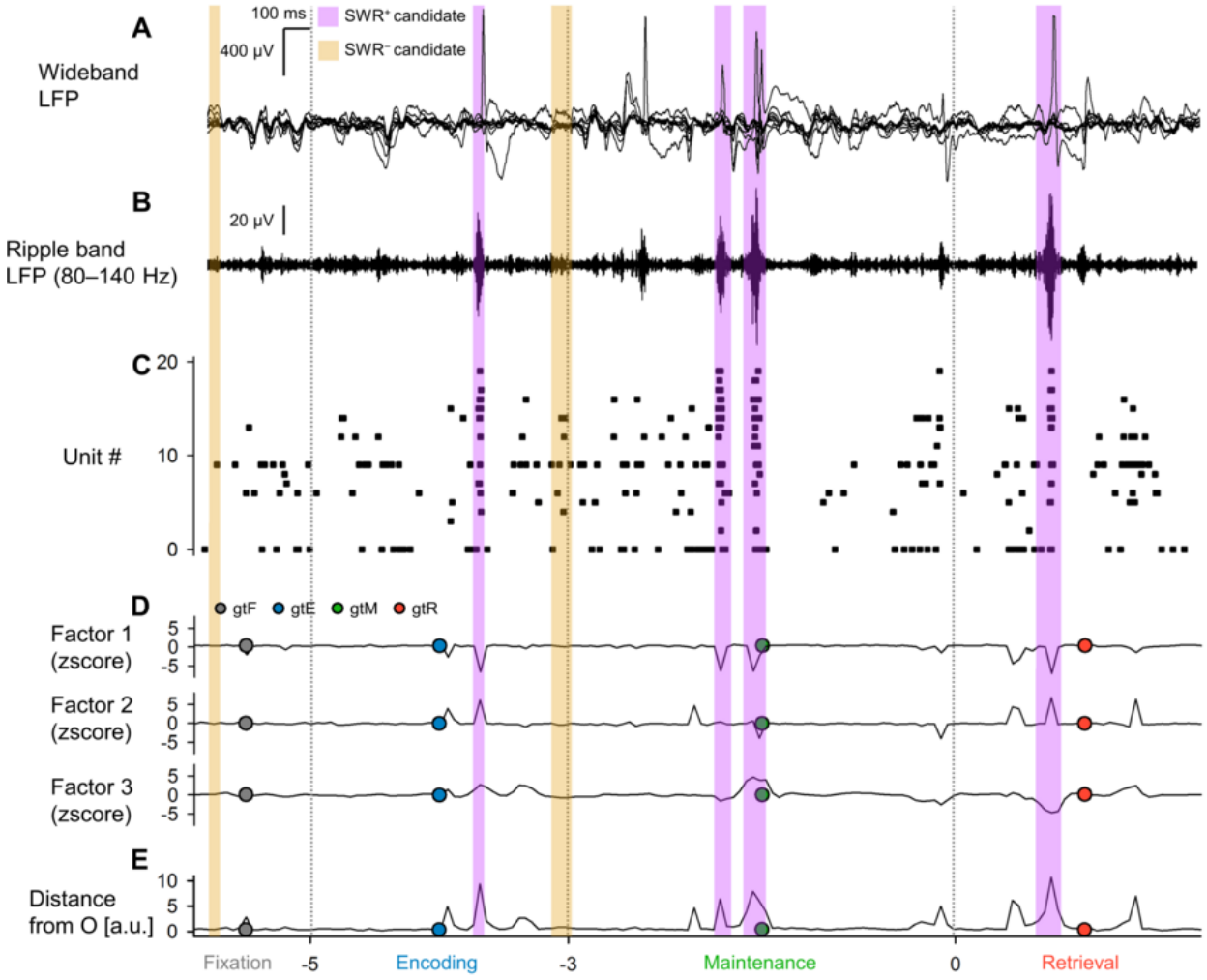

Figure 1 – Local Field Potentials (LFP), Multiunit Activity, and Neural Trajectories in the Hippocampus During a Modified Sternberg Task

A. These traces show representative wideband LFP intracranial EEG (iEEG) signals recorded from the left hippocampal head. The subject performed a modified Sternberg working memory task, which includes fixation (1 s, *gray*), encoding (2 s, *blue*), maintenance (3 s, *green*), and retrieval (2 s, *red*). ***B.*** We then present the corresponding ripple band LFP traces. ***C.*** The raster plot depicts multiunit spikes taken from the LFP traces, sorted using a spike algorithm [38]. ***D.*** Subsequently, we illustrate the neural trajectories, which are calculated by GPFA on spike counts per unit with 50-ms bins. Each phase's geometric median is marked by the dot circles. ***E.*** The trajectory's distance from the origin O is portrayed, with *purple* and *yellow* rectangles indicating the timings for SWR^+ candidates and SWR^- candidates (considered as controls for SWR^+), respectively.

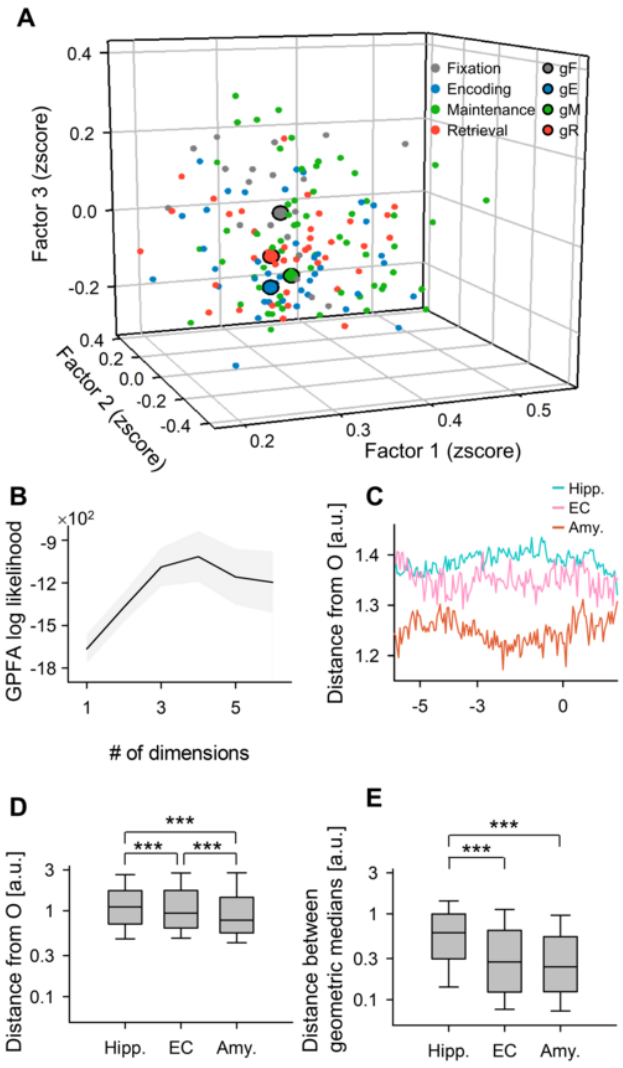

Figure 2 – State-Dependent Trajectories of Hippocampal Neurons

A. Neural trajectories within the initial three-dimensional factors derived from the Gaussian Process Factor Analysis (GPFA) are displayed. The smaller dots correspond to coordinates of 50-ms neural trajectory bins, while the larger dots with *black* edges signify the geometric medians for respective stages in the Sternberg working memory task: fixation (*gray*), encoding (*blue*), maintenance (*green*), and retrieval (*red*). ***B.*** The figure conveys the log-likelihood of the GPFA models versus the count of dimensions used to embed multiunit spikes found in the medial temporal lobe (MTL) territories. In specific, the elbow method pinpointed the optimal dimension to be three. ***C.*** This panel illustrates the distance of the neural trajectories from the origin (*O*) for the hippocampus (Hipp.), entorhinal cortex (EC), and amygdala (Amy.), against the time elapsed from the probe onset. ***D.*** The distance of the trajectory from *O* within MTL regions is displayed. The hippocampus shows the farthest distance, followed by the EC and the Amygdala. ***E.*** The plot represents inter-phase trajectory distances within the MTL regions. Abbreviations:

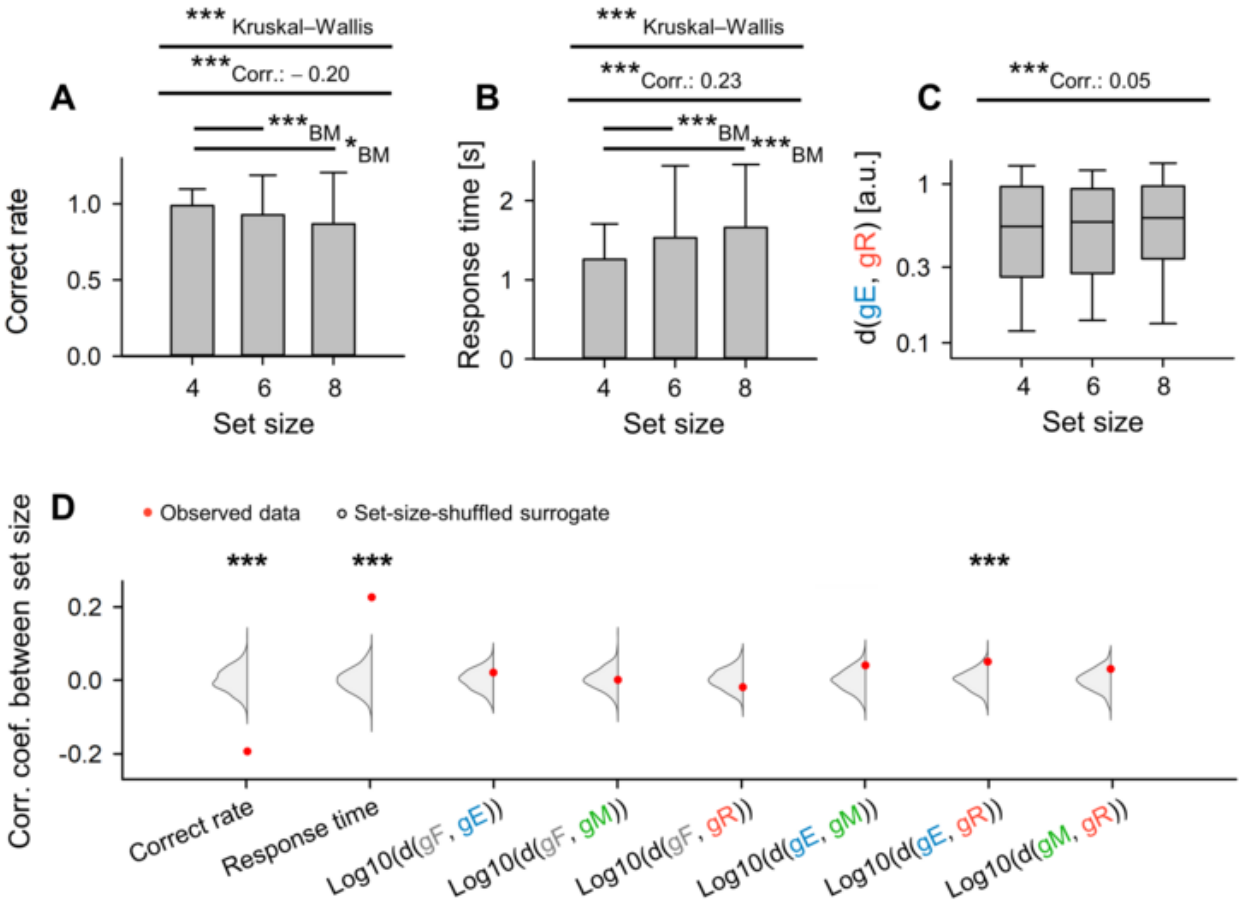

Figure 3 – Dependency of Trajectory Distance on Memory Load: Encoding and Retrieval States in Hippocampus

A. The relationship between set size (number of letters that need to be encoded) and correct rate in the working memory task (coefficient = −0.20, ***$p < 0.001$). ***B.*** The correlation between set size and response time (coefficient = 0.23, ***$p < 0.001$). ***C.*** The impact of set size on the inter-phase distances between the encoding and retrieval phases ($\|g_E g_R\|$) (correlation coefficient = 0.05). ***D.*** *Red* dots represent experimental observations of correlations between set size and the following parameters: correct rate, response time, $\log_{10}\|g_F g_E\|$, $\log_{10}\|g_F g_M\|$, $\log_{10}\|g_F g_R\|$, $\log_{10}\|g_E g_M\|$, $\log_{10}\|g_E g_R\|$, and $\log_{10}\|g_M g_R\|$. The *gray* kernel density plot illustrates the corresponding set-size-shuffled surrogate (n = 1,000) (***ps < 0.001).

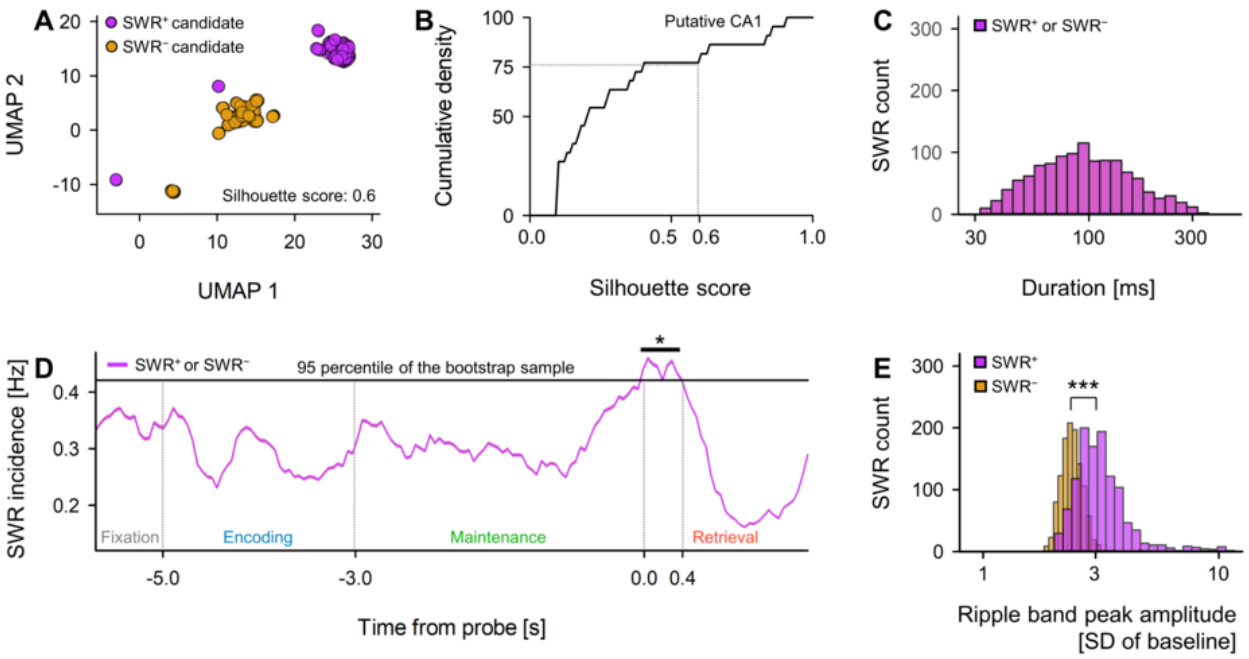

Figure 4 – Detection of SWRs in Presumptive CA1 Regions

A. Two-dimensional UMAP (Uniform Manifold Approximation and Projection) [41] projection of multiunit spikes during SWR^+ candidates (*purple*) and SWR^- candidates (*yellow*). ***B.*** Cumulative density plot shows silhouette scores, indicative of UMAP clustering quality, for hippocampal regions (see Table 2 for reference). Note that hippocampal regions with silhouette scores greater than 0.60 (equivalent to the 75^{th} percentile) were identified as possible CA1 regions. SWR^+ and SWR^- candidates recorded from these speculative CA1 regions were respectively classified as SWR^+ and SWR^- (*ns* = 1,170). ***C.*** The identical distributions of durations are presented for SWR^+ (*purple*) and SWR^- (*yellow*), owing to their definitions (93.0 [65.4] ms, median [IQR]). ***D.*** SWR incidence for both SWR^+ (*purple*) and SWR^- (*yellow*) obtained relative to the probe's timing is illustrated as a mean ±95% confidence interval. However, as the intervals may not be visible due to their narrow range, note that a significant increase in SWR incidence was detected during the initial 400 ms of the retrieval phase (0.421 [Hz], $*p < 0.05$, bootstrap test). ***E.*** The distributions of ripple band peak amplitudes for SWR^- (*yellow*; 2.37 [0.33] SD of baseline, median [IQR]) and SWR^+ (*purple*; 3.05 [0.85] SD of baseline, median [IQR]) are delineated ($***p < 0.001$, the Brunner–Munzel test).

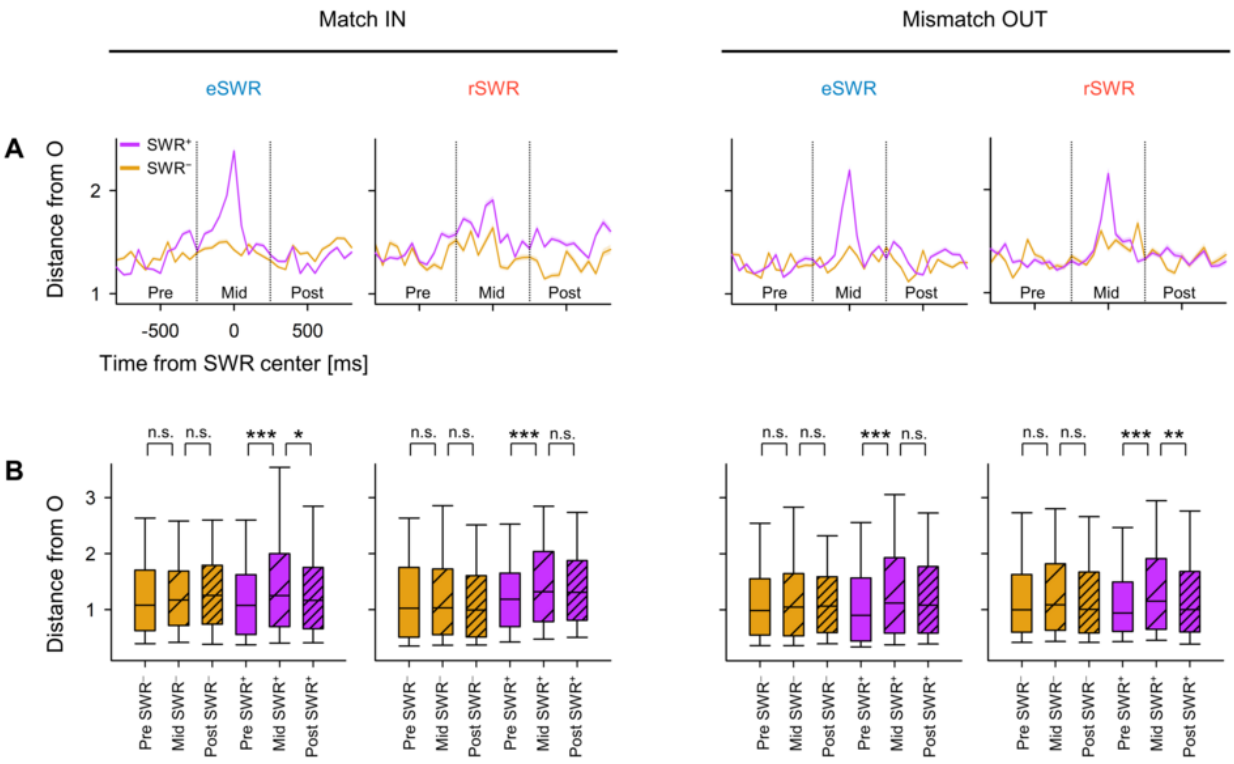

Figure 5 – Transient Alterations in Neural Trajectory During SWR Events

A. Displayed is the distance from origin (O) of the peri-sharp-wave-ripple trajectory (mean ±95% confidence interval). The intervals may not be apparent due to their slender ranges. ***B.*** Shown is the distance from the origin (O) during pre-, mid-, and post-SWR periods ($^*p < 0.05$, $^{**}p < 0.01$, $^{***}p < 0.001$; assessed using the Brunner–Munzel test). Abbreviations: SWR, sharp-wave ripple events; eSWR, SWR during the encoding phase; rSWR, SWR while in the retrieval phase; SWR^+, positive SWR event; SWR^-, control events for SWR^+; pre-, mid-, or post-SWR denote the time intervals from −800 to −250 ms, from −250 to +250 ms, or from +250 to +800 ms, all relative to the center of the SWR.

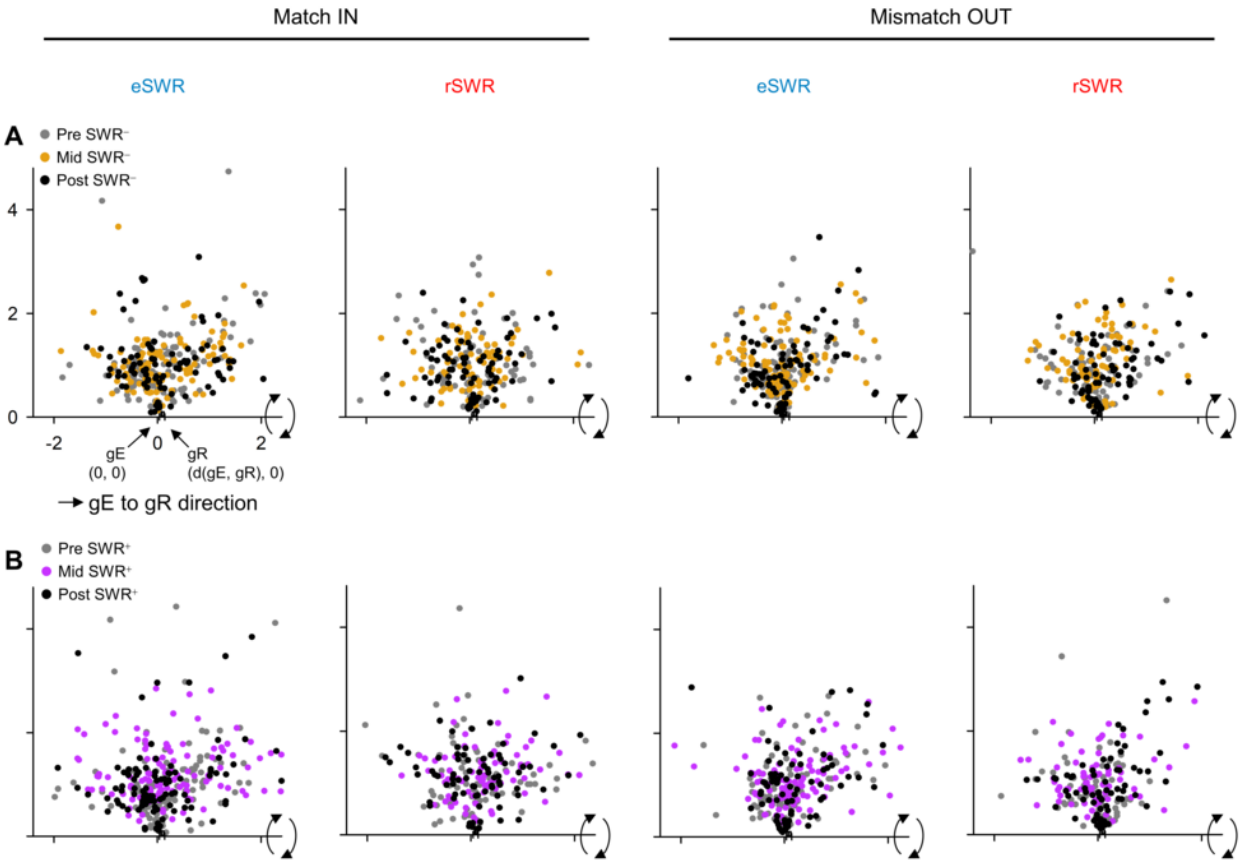

Figure 6 – Visualization of Neural Trajectories during SWR in Two-Dimensional Spaces

The panels display hippocampal neural trajectories during SWR as projected onto two-dimensional spaces. ***A.*** Indicates hippocampal neural trajectories pre-SWR$^-$ (*gray*), mid-SWR$^-$ (*yellow*), and post-SWR$^-$ (*black*). ***B.*** Represents the equivalents for SWR$^+$ as opposed to SWR$^-$. The $\|g_E g_R\|$ varied among sessions. The projection was applied in the following manner: First, a linear transformation positioned g_E at the origin O (0,0), and g_R at ($\|g_E g_R\|$, 0). The point cloud was then rotated around the $g_E g_R$ axis (equivalent to the x axis) for fitting into two-dimensional spaces. Therefore, within these two-dimensional spaces, both the distances from O and the angles preserved the original makeup of the $g_E g_R$ axis from the original three-dimensional spaces. Abbreviations: SWR signifies sharp-wave ripple events; eSWR denotes SWR during the encoding phase; rSWR indicates SWR during the retrieval phase; SWR$^+$, marks an SWR event; SWR$^-$ refers to control events for SWR$^+$; pre-SWR, mid-SWR, or post-SWR, reference the time intervals from −800 to −250 ms, from −250 to +250 ms, or from +250 to +800 ms from the center of SWR.

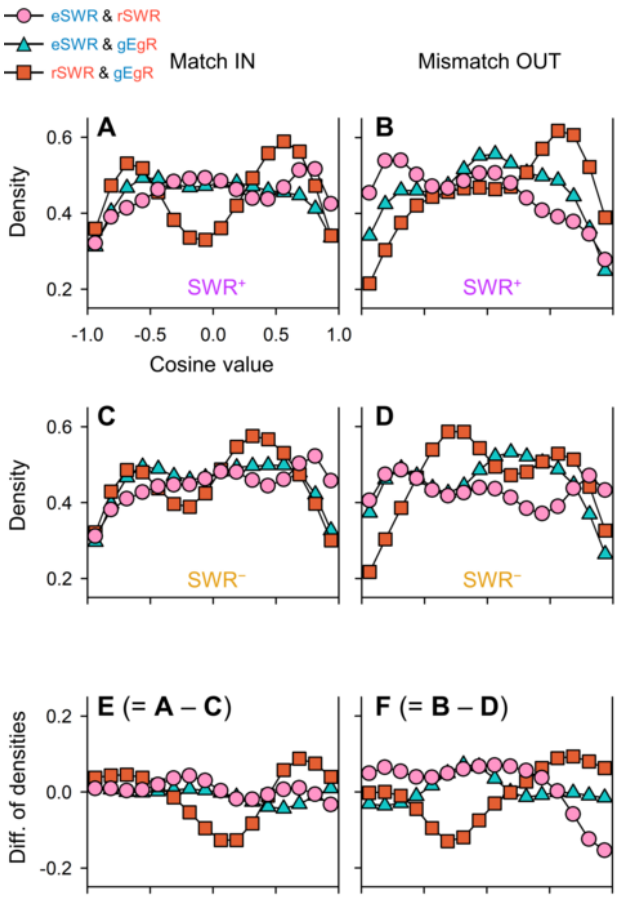

Figure 7 – Directions of Neural Trajectories during SWRs Based on Encoding and Retrieval States

A–B Kernel density estimation (KDE) distributions of $\overrightarrow{\mathrm{eSWR}^{+}} \cdot \overrightarrow{\mathrm{rSWR}^{+}}$ (*pink circles*), $\overrightarrow{\mathrm{eSWR}^{+}} \cdot \overrightarrow{\mathrm{g_E g_R}}$ (*blue triangles*), and $\overrightarrow{\mathrm{rSWR}^{+}} \cdot \overrightarrow{\mathrm{g_E g_R}}$ (*red rectangles*) in Match In (*A*) and Mismatch OUT tasks (*B*). ***C–D*** Present the corresponding distributions of SWR^{-} instead of those of SWR^{+} in *A* and *B*. ***E–F*** Depict the differences in the distributions of SWR^{+} and SWR^{-}, illuminating the SWR components ($E = C - A$; $F = D - B$). Note the biphasic distributions of $\overrightarrow{\mathrm{rSWR}^{-}} \cdot \overrightarrow{\mathrm{g_E g_R}}$, suggesting fluctuations between the encoding and retrieval states during the Sternberg task. Moreover, inverse directionality between $\overrightarrow{\mathrm{eSWR}^{+}}$ and $\overrightarrow{\mathrm{rSWR}^{+}}$ was observed (*pink circles*) in the Mismatch OUT task, but not in the Match IN task ***E–F***). Finally, shifts from the retrieval to encoding states were evident in the SWR components in both the Match IN and Mismatch OUT tasks (*red rectangles* in *E* and *F*).